© 2019. Published by The Company of Biologists Ltd | Journal of Cell Science (2019) 132, jcs232819. doi:10.1242/jcs.232819

RESEARCH ARTICLE

Identification and characterization of the land-plant-specific microtubule nucleation factor MACET4

Sharol Schmidt and Andrei Smertenko*

ABSTRACT

Here, we show that the embryophyte (land-plant)-specific protein MACERATOR4 (MACET4) binds microtubules *in vitro* and *in vivo*, promotes microtubule polymerization at sub-critical tubulin concentrations, decreases the lag phase in microtubule bulk polymerization assays, and colocalizes with microtubule nucleation sites. Furthermore, we find that MACET4 forms oligomers that induce aster formation *in vitro* in a manner that is similar to aster formation mediated by centrosomes and TPX2. MACET4 is expressed during cell division and accumulates at the microtubule nucleation regions of the plant-specific cytokinetic microtubule array, the phragmoplast. We found that MACET4 localizes to the preprophase band and the cortical division zone, but not the spindle. MACET4 appears as cytoplasmic foci *in vivo* and forms octamers *in vitro*. Transient expression in tobacco leaf pavement cells results in labeling of shrinking plus- and minus-ends. MACET4 facilitates microtubule depolymerization by increasing the frequency of catastrophes *in vivo* and by suppressing rescues *in vitro*. Microtubules formed in the presence of MACET4 *in vitro* are shorter, most likely due to the depletion of the free tubulin pool. Accordingly, MACET4 knockdown results in longer phragmoplasts. We conclude that the direct activity of MACET4 is in promoting microtubule nucleation.

This article has an associated First Person interview with the first author of the paper.

KEY WORDS: Phragmoplast, Microtubules, Nucleation, Cytokinesis

INTRODUCTION

Plant cytokinesis is executed by a highly specialized cellular machine, the phragmoplast (Bajer, 1968; Becker, 1938; Hepler and Jackson, 1968). A typical phragmoplast consists of two nearly parallel microtubule arrays that sandwich the midzone, where assembly of the partition between daughter cells or cell plate takes place (Bajer, 1968; Becker, 1938; Samuels et al., 1995; Segui-Simarro et al., 2004; Wasteneys, 2002). Microtubules function as a scaffold for structural support of the cell plate and for transporting cell plate-building materials. The phragmoplast initially forms between the daughter nuclei at the end of anaphase (Cutler and Ehrhardt, 2002; Ueda et al., 2003). Completion of cell plate synthesis promotes microtubule disassembly in this region. The microtubule structural protein, tubulin, is released during depolymerization and is then recycled for assembling new microtubules at the outer edge of the cell plate (Yasuhara et al., 1993). As phragmoplast diameter is generally smaller that the diameter of the cell, continuous microtubule polymerization, de-polymerization and re-polymerization drives phragmoplast expansion towards the cortical division zone located at the plasma membrane of the cell. Attachment of the cell plate to a site within the cortical division zone leads to phragmoplast disassembly.

Phragmoplast microtubules are twice as dynamic as interphase microtubules (Hush et al., 1994; Smertenko et al., 2011). One of the underlying reasons for this difference is continuous depolymerization of microtubules in the region where cell plate synthesis is accomplished and polymerization of microtubules on the phragmoplast outer edge. What drives the depolymerization remains unknown, but new microtubules in the phragmoplast are nucleated by the γ-tubulin ring complex (γ-TuRC; Hashimoto, 2013). Furthermore, phragmoplast microtubules are shorter than those in interphase. A higher frequency of transition from polymerization to depolymerization (catastrophe) could be responsible for both restricting microtubule elongation and for increasing microtubule dynamicity.

On the tree of life, the phragmoplast appears in Charophyceae algae, which gives rise to land plants (embryophytes) (Buschmann and Zachgo, 2016; Leliaert et al., 2011). This fact suggests that higher tissue complexity, which accompanied adaptation to terrestrial life, was facilitated by cytokinesis with the phragmoplast. However, whether expansion is the intrinsic phragmoplast feature remains debatable considering findings that within the Charophyceae family expansion has been observed in *Coleochaete orbicularis* (Cook, 2004), but not in *Chara zeylandica* (Cook et al., 1998).

Overall phragmoplast morphology resembles that of the animal cell cytokinetic structure, the midbody (Otegui et al., 2005). In particular, both structures are composed of two anti-parallel microtubule arrays that overlap at the midzone. However, the midbody lacks expansion and possesses a structurally stable midzone, whereas the phragmoplast midzone undergoes rapid reorganization (Samuels et al., 1995; Smertenko et al., 2018). The majority of known phragmoplast microtubule regulators play a conserved role in midbody functions (McMichael and Bednarek, 2013). Considering the unique nature of phragmoplast expansion, we hypothesized that plants must have evolved specific proteins to facilitate this process. To date, the only plant-specific microtubule-binding protein localized in the phragmoplast known is Tan1 (Cleary and Smith, 1998; Smith et al., 2001). In angiosperms, Tan1 is described to function in determining the cell division plane orientation (Rasmussen et al., 2011; Walker et al., 2007). We hypothesize there are additional plant-specific proteins that determine features of phragmoplast organization which need to be studied in order to understand and model plant cytokinesis.

Here, we characterized embryophyte-specific microtubule-binding phragmoplast protein MACERATOR4 (MACET4) (Schmidt and Smertenko, 2016). MACET4 expresses during cell division and localizes to the anaphase spindle poles and phragmoplast distal zones where microtubule nucleation takes place. Biochemical analysis demonstrates that MACET4 oligomerizes, promotes microtubule

Institute of Biological Chemistry, Washington State University, Pullman, WA 99164, USA.

*Author for correspondence (andrei.smertenko@wsu.edu)

A.S., 0000-0002-5078-4881

Received 3 April 2019; Accepted 1 May 2019

Journal of Cell Science (2019) 132, jcs232819. doi:10.1242/jcs.232819

nucleation and polymerization whilst inhibiting transition from depolymerization to polymerization (rescue). We propose that MACET4 oligomers promote microtubule nucleation and indirectly promote catastrophe by rapid depletion of the free tubulin pool in the cell.

RESULTS

MACET4 controls phragmoplast size

The *Arabidopsis* protein MACET4 (At1g23790; Schmidt and Smertenko, 2016) localizes to microtubules when transiently expressed in tobacco (*Nicotiana benthamiana*) leaf pavement cells (Fig. S1A). *MACET4* is part of a co-expression network with a key regulator of phragmoplast assembly, a member of the kinesin 7 family, *NACK1/Hinkel* (Fig. S1B), and with a key spindle assembly factor *TPX2*. The co-expression network of *MACET4*, *NACK1* and *TPX2* also includes known regulators of cell division including *MAP65*-3 (also known as *PLE*), the kinesins ATK5 and PAKRP1L, and cyclin B2. Conceivably, *MACET4* is a cell-cycle-regulated gene. To test this hypothesis, we expressed a *GUS* reporter gene under control of the *MACET4* promoter (Fig. 1). Peak GUS activity was detected in root and shoot meristems, lateral root primordia, young leaves, vasculature, developing stomata, pollen grains and young flowers. No discernible GUS activity was detected in differentiated leaves.

To test the localization of MACET4 during cell division, we expressed MACET4–GFP under the control of the ubiquitin promoter in tobacco BY-2 cells. However, transgenic lines could not be recovered, suggesting that overexpression of MACET4 was lethal. To overcome this problem, we expressed GFP–MACET4 under control of an estrogen-inducible promoter in BY-2 cells and found that MACET4 associates with cortical microtubules, the pre-prophase band and the phragmoplast, but remained cytoplasmic during metaphase (Fig. 2; Movie 1). MACET4 is recruited onto microtubules again during anaphase (Fig. 2). During cytokinesis, MACET4–GFP localized to the phragmoplast distal zones (Fig. 2).

Genome analysis of plants from different taxa revealed that MACET4 homologs are only found in embryophytes (Fig. S2), suggesting that MACET4 evolved as plants began to colonize land. To determine the functions of *MACET4*, we analyzed T-DNA knockout mutants (Fig. S3). Seedlings of *mce4-1* and Col-0 plants were grown at 8°C for 4 weeks. The root growth rate was not different (Fig. 3A); however, the root meristem zone was longer in *mce4-1* than in Col-0 (Fig. 3B). Considering localization of MACET4 during cytokinesis, we examined morphology of the phragmoplast in *mce4-1*. The overall phragmoplast morphology showed no discernible phenotype in *mce4-1*; however, the phragmoplast length, measured as the distance between edges of the opposite distal zones (Smertenko et al., 2017) was greater in *mce4-1* (Fig. 3C, D). This phenotype could be partially complemented by expressing *proMACET4*:*MACET4-GFP* in the *mce4-1* background (Fig. 3C,D).

Analysis of *mce4-1;proMACET4*:*MACET4-GFP* lines revealed localization of MACET4 in the preprophase band and the phragmoplast, but not in the spindle (Fig. 3E–G; Movies 2 and 3). We also detected signal in the cortical division zone (Fig. 3G, frame 548). Overall, the localization pattern in the phragmoplast in *A. thaliana* roots was similar to that in the BY-2 cells, with exception that labeling of anaphase spindle was restricted to the spindle poles (Fig. 3G, frame 476). Labeling of anaphase spindle microtubules in BY-2 cells could be the consequence of protein overexpression driven by the inducible promoter. The expression level in the interphase cells was below the sensitivity of our approach. Thus, MACET4 is a cell-cycle-regulated embryophyte-specific protein that controls phragmoplast size.

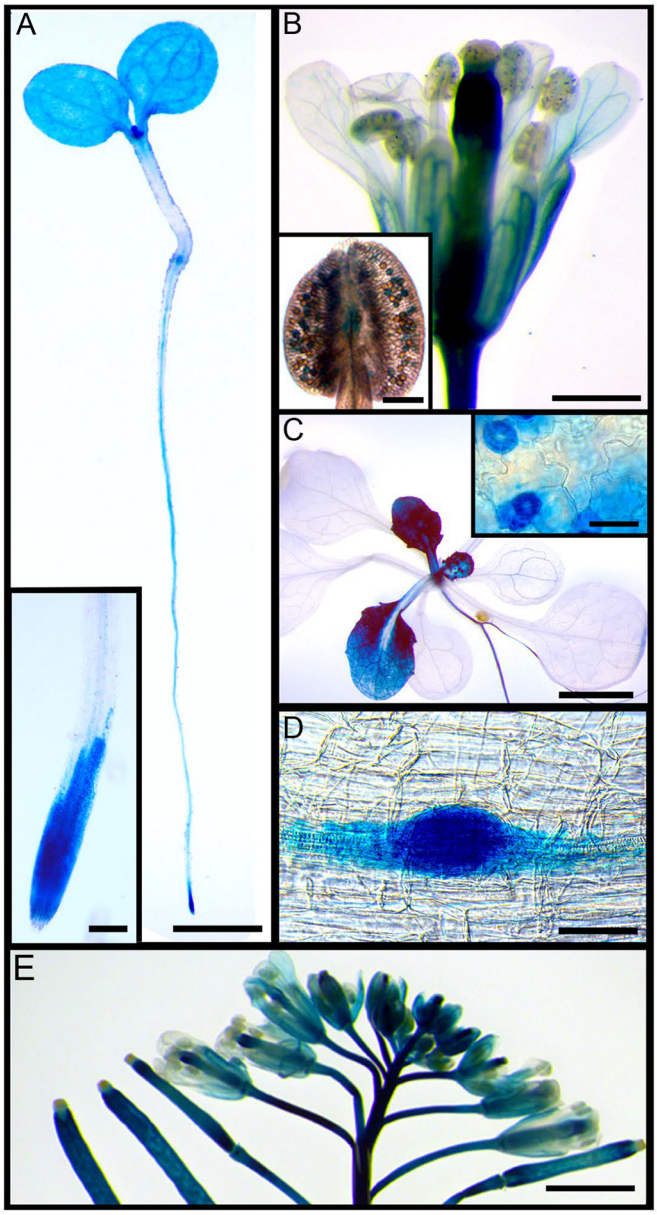

Fig. 1. GUS activity in the tissues and organs of transgenic *Arabidopsis* plants harboring a *proMACET4:GUS* gene fusion construct. (A) In the seedling, GUS activity, as a reporter for *MACET4* transcription, was strongest in the apical meristems and cotyledons. Scale bar: 2 mm. The inset shows a higher magnification of the root tip. Scale bar: 200 µm. (B) GUS activity, as a reporter for MACET4, in the flower. Scale bar: 1 mm. The inset shown GUS activity in pollen grains. Scale bar: 50 µm. (C) The strongest GUS activity was observed in the young leaves. Differentiated leaves lack discernible activity. Scale bar: 2 mm. The inset shows strong signal in the newly formed stomata. Scale bar: 50 µm. (D) High GUS activity in lateral root primordia. Scale bar: 100 µm. (E) GUS activity in the flower rosette. Scale bar: 3 mm.

Impact of MACET4 on microtubule dynamics *in vivo*

The longer phragmoplasts in *mce4-1* indicates that MACET4 contributes to regulating microtubule dynamics during cytokinesis. However, resolving the behavior of individual microtubules in the phragmoplast remains technically impossible due to the high concentration of free tubulin in this region (Vyplelová et al., 2018). Instead, we analyzed microtubule dynamics in leaf pavement cells of tobacco plants stably expressing *Arabidopsis* β6-tubulin–mCherry under the control of the CaMV35S promoter (Abe and

Journal of Cell Science (2019) 132, jcs232819. doi:10.1242/jcs.232819

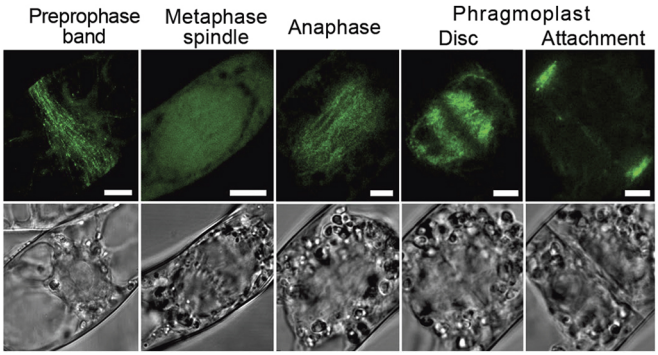

Fig. 2. Localization of MACET4 during cell division. Bright field and GFP signal in BY2 cells stably transformed with *pro*XVE:GFP-MACET. Scale bars: 5 µm.

Hashimoto, 2005). Expression of MACET4–GFP under control of the strong *UBI10* promoter results in dense labeling of microtubules (Fig. 4A), which is different from the GFP puncta observed in the phragmoplast (Fig. 2; Fig. 3E–G). In an attempt to mimic the phragmoplast localization, we expressed MACET4–GFP under control of native promoter (*proMACET4*:*MACET4-GFP*). This approach was successful resulting in the GFP puncta localized along the microtubules and in the cytoplasm (Fig. 4A). We used both approaches to determine the impact of MACET4 on microtubule dynamics.

Detailed analysis of *proMACET4*:*MACET4-GFP* cells showed two patterns of GFP puncta association with the microtubule lattice: transient (<30 s) or persistent (>30 s). All persistent associations coincided with the microtubule crossover sites (n=50; Fig. 4B). Furthermore, all microtubule plus-end depolymerization events (n=43) were accompanied by the enrichment of GFP signal at the depolymerizing tip (Fig. 4B; Fig. S4A, Movie 4). Shrinking minus-ends of 'treadmilling' microtubules also accumulated MACET4–GFP (Fig. S4B,C). Enrichment of MACET4–GFP signal preceded cytoplasmic microtubule nucleation events (Fig. 4C; Movie 5) and coincided with the sites of branching microtubule nucleation (Fig. 4D; Movie 6). We found that all microtubule nucleation events under our experimental conditions occurred at sites enriched with MACET4 (n=12).

To measure the impact of MACET4 on microtubule dynamics, we artificially colored growing and shrinking microtubule ends using a published technique (Lindeboom et al., 2013). Growing and shrinking microtubules were apparent in both control and cells transfected with *proMACET4*:*MACET4-GFP*, but not in cells transfected with *proUBN10*:*GFP-MACET4* (Fig. 4E; Movies 7 and 8). In the latter case, microtubules appeared to be stable and the only type of dynamics was wavering (Fig. 4E; Fig. S4D, Movie 9). Treatment of cells with an inhibitor of microtubule polymerization amiprophos methyl (APM) caused depolymerization of microtubules in the control, but microtubule fragments persisted in cells constitutively expressing MACET4 (Fig. S4E). Hence, overexpression of MACET4 stabilizes microtubule *in vivo* through the inhibition of catastrophe events.

Analysis of microtubule dynamics in cells transfected with *proMACET4*:*MACET4-GFP* showed that MACET4 reduces microtubule polymerization and depolymerization rates (Fig. 4F). Furthermore, MACET4 caused a greater frequency of depolymerizing microtubules (Fig. 4F; Fig. S4G) while not affecting the frequency of microtubule polymerization events (Fig. S4F). MACET4 also promoted the transition from polymerization to pause, from pause to catastrophe, and from polymerization to catastrophe. At the same time, transitions from catastrophe to polymerization and from catastrophe to pause were greater in these cells than in the control. Therefore, ectopic expression of MACET4 under control of native promoter, which results in lower levels of protein expression relative to that mediated by strong constitutive expression, causes a shift of bulk microtubule dynamics towards depolymerization.

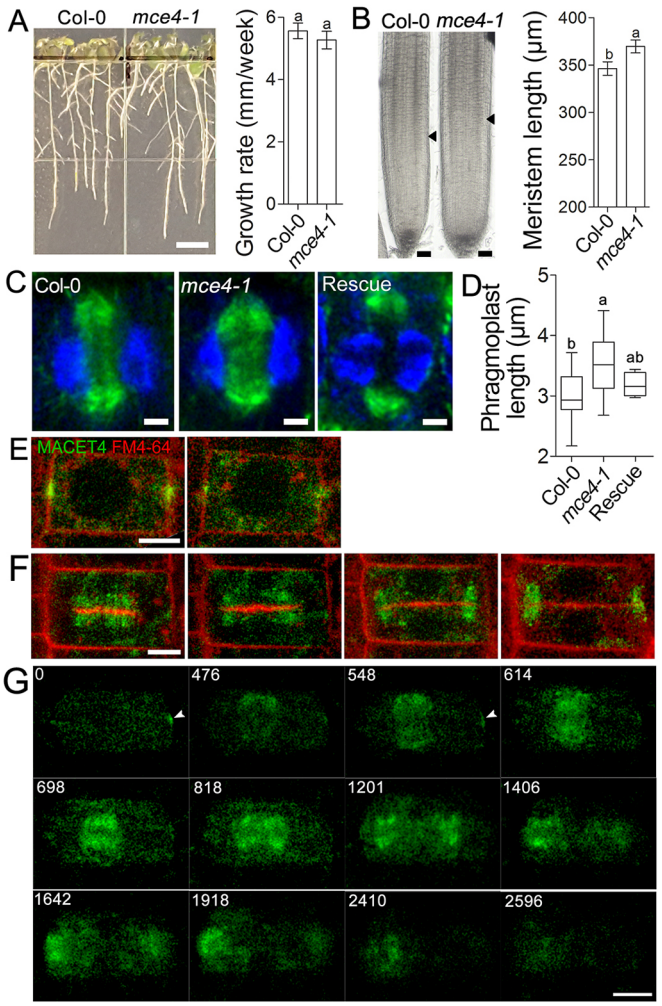

Fig. 3. MACET4 controls phragmoplast size. (A) Representative images of roots and quantification (mean±s.d.) of root growth rate in Col-0 and *mce4-1* seedlings at week 3 after germination when grown at 8°C. Scale bar: 5 mm; n=30. (B) Representative images of roots and quantification (mean±s.d.) of the length of the root apical meristem, showing that it is longer in *mce4-1* strains. Scale bars: 50 µm; n=30. (C,D) Representative images of the phragmoplast (C) and quantification (D) showing it is longer in the *mce4-1* strain; *proMACET4:MACET4* partially rescues this phenotype. Scale bars: 2 µm. Five phragmoplasts in each three independent plants were measured in D (n=15). The box represents the 25–75th percentiles, and the median is indicated. The whiskers show the range. (E,F) Localization of MACET4–GFP in the pre-prophase band (PPB) (E) and in the phragmoplast (F) in apical root meristem cells following staining of plasma membrane and cell plate with FM4-64. Scale bars: 5 µm. (G) Localization of the MACET4–GFP during cell division, starting from the PPB stage and until completion of cytokinesis. The arrowhead shows GFP signal at the PPB. This signal persists until phragmoplast formation at time 548. Scale bar: 5 µm. Numbers indicate relative time in seconds. Different letters in panels A, B and D indicate values that are statistically different from one another (P<0.05; unpaired t-test in A and B, one-way ANOVA in D).

Journal of Cell Science (2019) 132, jcs232819. doi:10.1242/jcs.232819

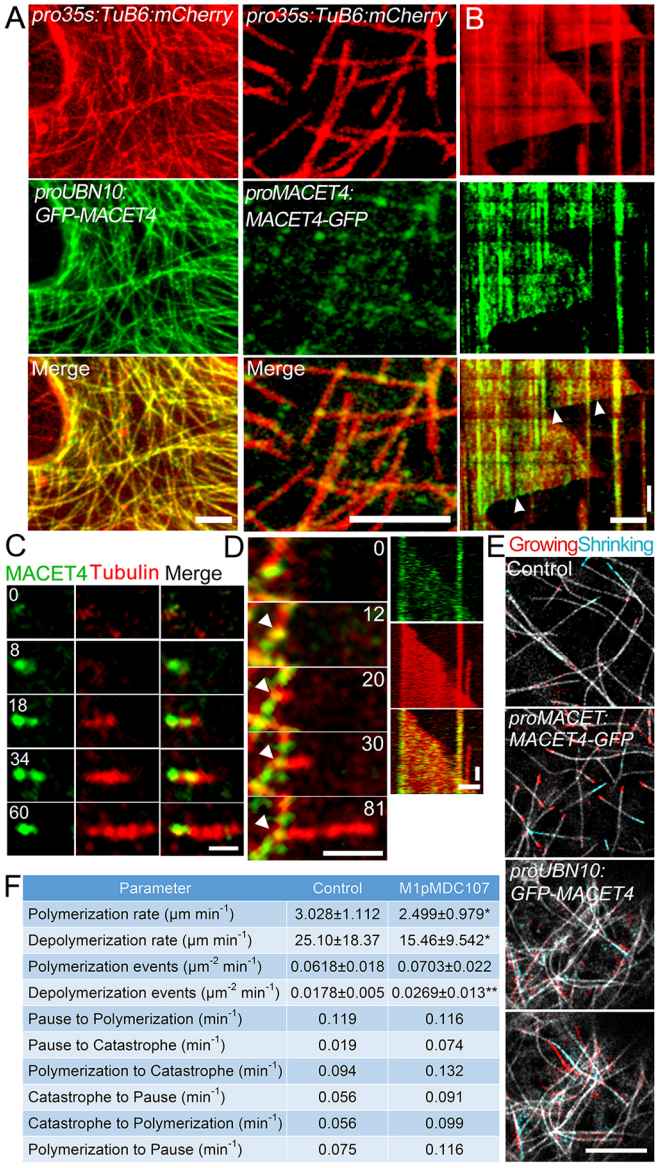

F

Parameter	Control	M1pMDC107
Polymerization rate (μm min^{-1})	3.028±1.112	2.499±0.979*
Depolymerization rate (μm min^{-1})	25.10±18.37	15.46±9.542*
Polymerization events (μm^{-2} min^{-1})	0.0618±0.018	0.0703±0.022
Depolymerization events (μm^{-2} min^{-1})	0.0178±0.005	0.0269±0.013**
Pause to Polymerization (min^{-1})	0.119	0.116
Pause to Catastrophe (min^{-1})	0.019	0.074
Polymerization to Catastrophe (min^{-1})	0.094	0.132
Catastrophe to Pause (min^{-1})	0.056	0.091
Catastrophe to Polymerization (min^{-1})	0.056	0.099
Polymerization to Pause (min^{-1})	0.075	0.116

Fig. 4. Effect of MACET4 on microtubule dynamics *in vivo*. (A) MACET4 decorates microtubules when expressed under the control of a constitutive promoter (*proUBN*), whereas expression under native promoter (*proMACET*) results in puncta along the microtubules. Scale bars: 5 µm. (B) Kymograph of a dynamic microtubule in a cell transfected with *proMACET4:MACET4-GFP*. Vertical scale bar, 1 min; horizontal scale bar, 5 µm. The arrowheads highlight localization of MACET4–GFP at the shrinking plus-end. (C) Selected time-lapse frames showing that MACET4–GFP (expressed via *proMACET4: MACET4-GFP*, green) localizes to the cytoplasmic microtubule nucleation site. Scale bar: 1 µm. Numbers indicate relative time in seconds. (D) As in C, with selected frames and a kymograph showing MACET4-GFP at a microtubule nucleation site on the microtubule lattice. Horizontal scale bars, 2 µm; vertical scale bars, 30 s. Numbers indicate relative time in seconds. Tubulin is shown in red in A–D. (E) Coloring growing microtubules in red and shrinking microtubules in cyan reveals suppression of microtubule dynamics upon constitutive expression of MACET4. Scale bar: 10 µm. (F) Microtubule dynamic parameters (mean±s.d. where given) in control and *proMACET4: MACET4-GFP*-expressing (M1pMDC107) cells. *P<0.02, **P=0.0006 compared with the control (unpaired *t*-test). The experiment was replicated twice (n>15 measurements in each).

MACET4 is a microtubule-binding protein

Although MACET4 colocalizes with microtubules in cells (Fig. 4A,B), this interaction could be indirect through another microtubule-binding protein. To test whether MACET4 binds microtubules directly, we performed a co-sedimentation assay with recombinant MACET4 and Taxol-stabilized microtubules. MACET4 was recovered in the pellet with microtubules, whereas without microtubules it remained in the supernatant (Fig. 5A). Hence, MACET4 is a true microtubule-binding protein.

Next, we determined the impact of MACET4 on microtubule polymerization by performing a turbidimetric assay. MACET4 increased the density of a tubulin solution in a concentration-dependent manner (Fig. S5A). Light-absorbance of a tubulin solution could increase due to microtubule polymerization, bundling or both. To distinguish between these possibilities, we measured the impact of MACET4 on bulk microtubule polymer production by performing a sedimentation assay. Different concentrations of MACET4 were added to a tubulin solution and incubated at 35°C for 20 min. The polymer was recovered by centrifugation and analyzed by SDS-PAGE (Fig. S5B). We found that the amount of microtubules in the pellet increased in a MACET4 concentration-dependent manner (Fig. S5C). This result demonstrates the ability of MACET4 to promote tubulin polymerization.

To test the bundling activity, we examined the effect of MACET4 on microtubules polymerized with ATTO488-labeled tubulin. Without MACET4 we observed formation of individual microtubules, whereas addition of MACET4 to the polymerization reaction caused formation of asters (Fig. 5B). Furthermore, the presence of MACET4 resulted in shorter individual microtubules relative to the control (Fig. 5C). The ability to induce formation of shorter microtubules in these assays prompted At1g23790 to be named MACERATOR4 (MACET4). However, we have no evidence that MACET4 reduces microtubule length through severing. Instead, microtubule elongation is likely to be inhibited by depleting free tubulin in the reaction. In this way, MACET4 increases the bulk of microtubule polymer while restricting elongation of individual microtubules.

The fact that MACET4 can induce asters, taken together with colocalization to the cytoplasmic microtubule nucleation sites *in vivo* (Fig. 5C), suggests that MACET4 possesses microtubule nucleation activity. To test this hypothesis, we created stable microtubule 'seeds' with ATTO488-labeled tubulin polymerized with the non-hydrolyzable GTP analog GMPCPP. We then mixed 5 µM Rhodamine-labeled tubulin with the 'seeds' and allowed the microtubules to polymerize. Tubulin concentration was optimized to prevent spontaneous microtubule nucleation but to allow polymerization on the seeds (Fig. 5D). In the presence of MACET4, 32% of microtubules formed *de novo* (defined as microtubule nucleation events that occur independently of the seed) relative to 0% in the control supplemented with MACET4 dialysis buffer (Fig. S5D). Furthermore, every seed in the presence of MACET4 had a microtubule extension, whereas as many as 28% of the seeds in the control reactions exhibited no microtubule extensions (Fig. S5E). Therefore, MACET4 promotes microtubule nucleation at subcritical concentrations of tubulin and facilitates microtubule elongation.

MACET4-induced asters resemble those generated from centrosomes. However, centrosomes promote nucleation of microtubules by recruiting multiple γ-tubulin ring complexes (γ-TuRCs) each consisting of many subunits. In gel-filtration chromatography experiments, MACET4 eluted just before the 443 kDa marker (Fig. 5E). Considering predicted molecular weight of 57 kDa, this approximately corresponds to the octamer, which is smaller than a γ-TuRC. To explain this observation we hypothesized that MACET4 facilitates aster formation by bundling early nucleation intermediates. To test this hypothesis we added MACET4 to a

Journal of Cell Science (2019) 132, jcs232819. doi:10.1242/jcs.232819

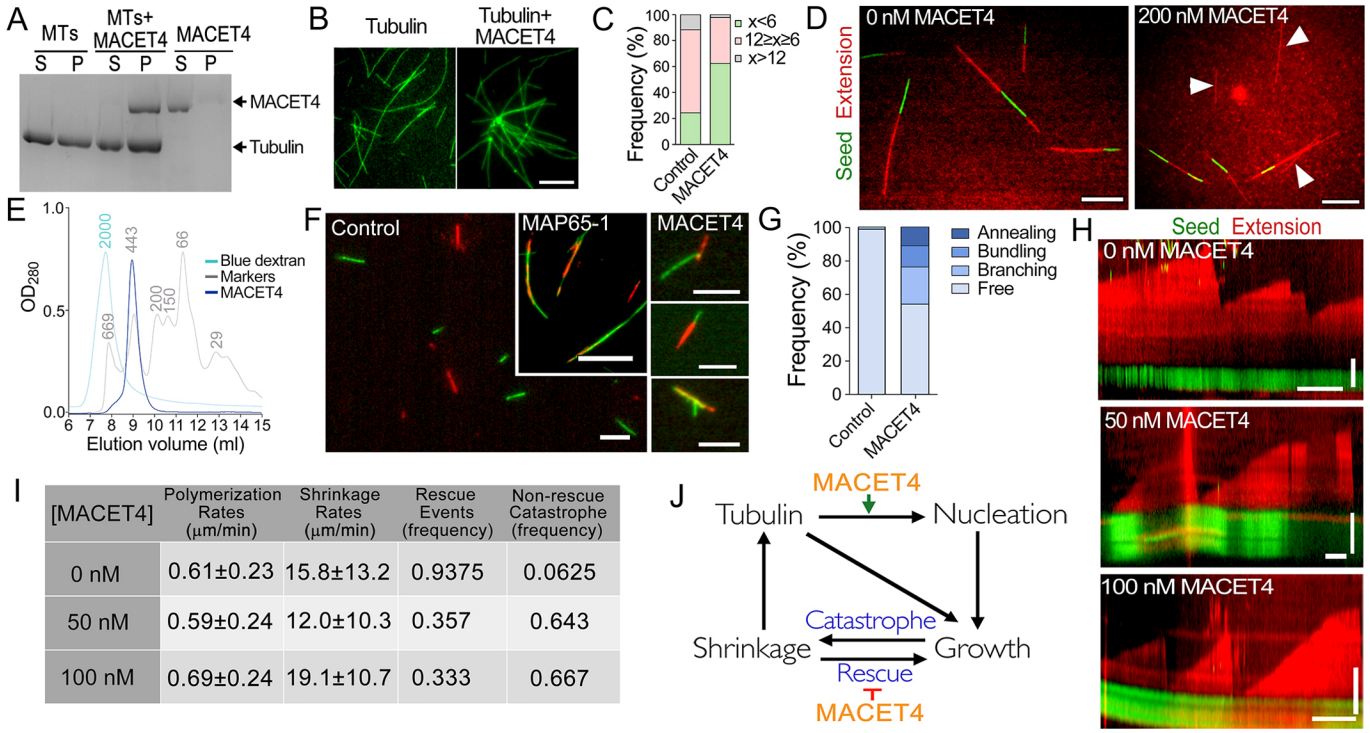

[MACET4]	Polymerization Rates (μm/min)	Shrinkage Rates (μm/min)	Rescue Events (frequency)	Non-rescue Catastrophe (frequency)
0 nM	0.61±0.23	15.8±13.2	0.9375	0.0625
50 nM	0.59±0.24	12.0±10.3	0.357	0.643
100 nM	0.69±0.24	19.1±10.7	0.333	0.667

Fig. 5. MACET4 is a microtubule-associated protein that promotes polymerization and nucleation *in vitro*. (A) MACET4 co-sediments with Taxol-stabilized microtubules, but remains in the supernatant without microtubules. S, supernatant; P, pellet. (B) MACET4 induces aster formation with ATTO488-labeled tubulin. Scale bar: 2 µm. (C) Frequencies of microtubule lengths (measured in µm) in reactions containing MACET4 or the dialysis buffer (Control). P<0.0001 (unpaired t-test; control, n=111; MACET4, n=264). (D) MACET4 promotes nucleation of microtubules (red) independently of seeds (arrowheads) and also facilitates microtubule elongation on the stable seeds (green). Scale bars: 5 µm. (E) Elution profile of MACET4 from the gel-filtration column. The MACET4 peak appears just before the 443 kDa standard. (F) Recombinant MACET4 induces three types of interaction between the 'green' and 'red' seeds: brunching attachment, annealing and bundling. Microtubule seeds do not interact in the control reactions. Inset in the Control shows bundles formed upon addition of the known *Arabidopsis*-bundling protein MAP65-1. Scale bars: 5 µm in the Control and MACET4 images, 10 µm in MAP65-1 image. (G) Frequency of interactions in the Control and MACET4 reactions counted from images as in F. The chart shows mean values of three independent experiments (n=247 for control and n=298 for MACET4). (H) Kymographs show inhibition of rescue in the microtubule polymerization reactions containing the indicated concentration of MACET4. Horizontal scale bar, 90 s; vertical scale bar, 2 µm. (I) Parameters of microtubule dynamics from *in vitro* polymerization experiments. Results are mean±s.d. (J) Schematic showing how MACET4 promotes microtubule nucleation and inhibits rescue.

mixture of stable 'seeds' made with Rhodamine-labeled or ATTO488-labeled tubulin. Compared to the control reactions, addition of MACET4 caused three types of interactions between microtubules: parallel, branching and annealing (Fig. 5F,G). A known microtubule-bundling protein, MAP65, was used as a positive control, and induced formation of bundles distinct from those formed with MACET4. This outcome implies that MACET4 promotes aster formation through bundling of early microtubule nucleation intermediates, as MACET4-mediated bundling is reminiscent of asters rather than elongated bundles as seen with MAP65.

Although nucleation and branching activities provide a mechanism for the aster formation, understanding why microtubules formed in the presence of MACET4 are shorter required measurements of microtubule dynamics *in vitro*. In these experiments, we polymerized microtubules from Rhodamine-labeled tubulin on ATTO488-labeled seeds and followed microtubule dynamics. Kymographs showed that in the presence of MACET4, microtubules depolymerize down to the seed, whereas in the control reactions, rescues were common (Fig. 5H). Quantification of the kymographs demonstrates that MACET4 at the concentration 50 nM or 100 nM does not affect microtubule polymerization or depolymerization rates, but reduced the frequency of rescue by almost 3-fold (Fig. 5I). Therefore, MACET4 promotes microtubule nucleation and restricts microtubule elongation (Fig. 5J).

Mechanism of MACET4 binding to microtubules

The primary structure of MACET4 lacks any known functional domains. The predicted secondary structure consists primarily of random coil with several α-helical regions (Fig. 6A). Alignment of MACET4 homologs from angiosperms, gymnosperms and mosses revealed three conserved regions (I, II and III) that coincide with α-helical regions (Fig. 6B). We tested whether one of these regions is a microtubule-binding domain by producing fragments of MACET4 that include either N-terminal conserved region I (amino acid residues 1–127) or C-terminal conserved regions II and III (amino acid residues 287–518).

Co-sedimentation assays with taxol-stabilized microtubules demonstrated that both regions are capable of binding microtubules (Fig. 6C). All MACET4$^{287\text{-}518}$ in the reaction mixture was recovered in the pellet with microtubules and no protein was detected in the supernatant, whereas some of MACET4$^{1\text{-}127}$ remained in the supernatant. Consistently with this outcome, transient expression experiments in *N. benthamiana* cells showed that whilst MACET4$^{287\text{-}518}$ associated with microtubules, GFP-MACET4$^{1\text{-}127}$ was cytoplasmic (Fig. 6D). This means the main microtubule-binding region of MACET4 encompasses the C-terminal conserved motifs.

To determine the functions of MACET4$^{1\text{-}127}$ and MACET4$^{287\text{-}518}$ domains, we tested their activities *in vitro*. Turbidimetric assays revealed that MACET4$^{287\text{-}518}$ increases the optical density of the

Journal of Cell Science (2019) 132, jcs232819. doi:10.1242/jcs.232819

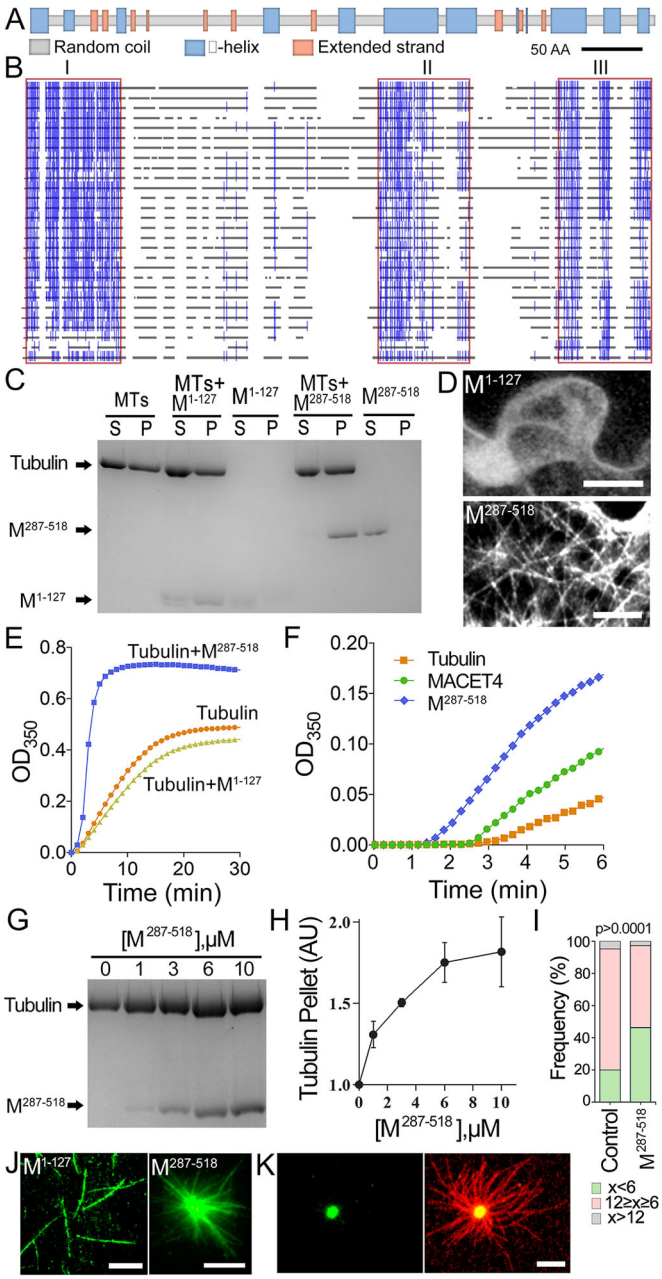

Fig. 6. The C-terminal region defines MACET4 activity. (A) Predicted secondary structure of MACET4. (B) Alignment of sequences from MACET family proteins from different species reveals three highly conserved regions (I, II and III); blue, conserved residues; gray, non-conserved residues; space, gaps. (C) SDS-PAGE gel of a microtubule co-sedimentation assay performed with peptides corresponding to MACET4 regions II+III ($M^{287–518}$) or region I ($M^{1–127}$). (D) GFP–$MACET4^{1–127}$ is cytoplasmic, whereas $MACET4^{287–518}$ localizes to microtubules. Scale bar: 5 µm. (E) Turbidimetric assays showing that $M^{287-518}$ increases turbidity of tubulin solution, whereas M^{1-127} lacks discernible activity. (F) Addition of full-length MACET4 or $M^{287-518}$ leads to a shorter lag-phase in the turbidimetric assays. Experiments in E and F were replicated three times. (G) $M^{287-518}$ co-sediments with polymerized tubulin in concentrations ranging from 1 to 10 µM. (H) $M^{287-518}$ promotes tubulin polymer formation in a concentration-dependent manner. Results are mean±s.d.; n=3. (I) Microtubules polymerized in the presence of $M^{287-518}$ are shorter. x represents the length in µm. P<0.0001 (control, n=230; $M^{287-518}$, n=227). (J) $M^{287-518}$, but not M^{1-127}, causes aster formation when incubated with fluorescently labeled tubulin. Scale bars: 5 µm. (K) A core of $M^{287-518}$ and ATTO488–tubulin nucleates microtubules from a Rhodamine and tubulin mix. Scale bar: 2.5 µm.

tubulin solution, whereas $MACET4^{1-127}$ lacked any discernible activity relatively to the control (Fig. 6E). Furthermore, the lag phase of tubulin as measured by assessing the optical density at 350 nm (OD_{350}) was shorter in the presence of $MACET4^{287-518}$ relative to full-length MACET4 or control (Fig. 6F). A shorter lag phase indicates the ability of the C-terminal region to promote microtubule nucleation and that the C-terminal region has enhanced function in the absence of the N-terminal region.

Measurements from the bulk microtubule polymer assay revealed that $MACET4^{287-518}$ promoted tubulin polymerization in a concentration-dependent manner (Fig. 6G,H). $MACET4^{287-518}$, but not $MACET4^{1-127}$, caused microtubule aster assembly (Fig. 6J). Microtubules in the asters originate from a bright central core, which seemingly functions similar to a centrosome in animal cells. We attempted to produce the cores by mixing 1 µM $MACET4^{287-518}$ with 5 µM ATTO488–tubulin. Supplementing this reaction with 10 µM Rhodamine–tubulin produced red asters on the green cores (Fig. 6K). No cores formed in the reactions containing ATTO488–tubulin alone. The proportion of short microtubules was greater in the reactions containing $MACET^{287-518}$ relative to the control (Fig. 6I). Taken together, these data indicate that: (1) the conserved C-terminal region of MACET4 possesses all activities of full-length MACET4, (2) the N-terminal region dampens activity of the C-terminal region, and (3) MACET4 and tubulin form microtubule-nucleating centers.

DISCUSSION

All thus far known microtubule-associated proteins in the phragmoplast are also found in animals. The only exception is Tan1, which directly binds microtubules (Smith et al., 2001) and cooperates with another microtubule-binding protein AIR9 in maintaining cell division plane orientation (Martinez et al., 2017). The role of Tan1 in the regulation of phragmoplast microtubule dynamics and its contribution to the evolution of phragmoplast remains to be determined. Here, we identify an embryophyte-specific microtubule-binding protein in the phragmoplast, called MACET4 (Schmidt and Smertenko, 2016). This finding, taken together with our knowledge about Tan1, supports the hypothesis that phragmoplast evolution required unique plant microtubule regulators.

Functional characterization demonstrates that MACET4 promotes microtubule polymerization at a concentration of tubulin that is incapable of self-nucleation *in vitro* and decreases the lag phase of microtubule polymerization in the turbidimetric assays. We also found colocalization of MACET4 with all free and lattice-associated microtubule nucleation sites *in vivo*. Taken together, MACET4 appears to be a microtubule-nucleation factor.

Microtubule nucleation in the phragmoplast was shown to be facilitated by the evolutionarily conserved γ-TuRC, which comprises six main subunits, GCP1–GCP6 (γ-tubulin is GCP1) and several associated proteins (Hashimoto, 2013). γ-TuRC nucleates microtubules preferentially on the lattice of existing microtubules, resulting in the formation of a branched microtubule network (Hashimoto, 2013). The knockout of both genes encoding γ-tubulin in *Arabidopsis* results in gametophytic lethality (Pastuglia et al., 2006) demonstrating functional non-redundancy of this nucleation pathway. By contrast, knockout of MACET4 results in a mild phenotype, which suggests either a non-essential role of MACET4 in microtubule nucleation or functional redundancy of MACET4 with its close homolog MACET5. Detailed characterization of *MACET4* and *MACET5* double-knockout mutants would provide more insights on the role of MACET4 *in vivo*.

Animals have an alternative to the γ-TuRC microtubule nucleation mechanisms. One of them relies on ‘targeting protein

Journal of Cell Science (2019) 132, jcs232819. doi:10.1242/jcs.232819

for *Xenopus laevis* kinesin-like protein 2' (TPX2; Gruss et al., 2001; Wittmann et al., 1998). TPX2 promotes microtubule nucleation during metaphase spindle assembly by reducing the rate of dissociation for tubulin subunits, thus stabilizing early nucleation intermediates (Reid et al., 2016; Roostalu et al., 2015; Wieczorek et al., 2015). Despite a different primary structure, the secondary structure of TPX2 and MACET4 consists of several predominantly α-helical domains interspersed by unstructured regions. Both TPX2 and MACET4 can nucleate microtubules and induce aster formation in a solution of purified tubulin (Brunet et al., 2004; Schatz et al., 2003). Plants have a TPX2 that binds microtubules of the mitotic spindle and plays a key role in spindle assembly (Vos et al., 2008). However, TPX2 does not bind microtubules during cytokinesis. By contrast, MACET4 does not bind microtubules in the mitotic spindle. This means plants could exploit distinct microtubule-nucleation mechanisms for assembling the mitotic spindle or the phragmoplast.

Another evolutionarily conserved microtubule nucleation mechanism relies on XMAP215 (also known as Stu2, chTOG and Alp14 and CKAP5 in various systems). This protein promotes microtubule polymerization and nucleation both *in vitro* and *in vivo*, and localizes to the microtubule nucleation sites and centrosomes in yeast and animal cells (Flor-Parra et al., 2018; Gunzelmann et al., 2018; Roostalu et al., 2015; Thawani et al., 2018; Wieczorek et al., 2015). XMAP215, like MACET4, also combines microtubule nucleating and polymerization activities, but the plant XMAP215 homolog MOR1 (also known as GEM1) binds along phragmoplast microtubules (as opposed to the puncta seen for MACET4) and localizes to the midzone (Kawamura et al., 2006; Twell et al., 2002). Distinct localization patterns indicate that MOR1 and MACET4 perform different functions during cytokinesis.

Both XMAP215 (including homologs from other systems) and TPX2 cooperate with γ-TuRC in promoting microtubule nucleation: TPX2 binds γ-tubulin through a conserved C-terminal domain whereas the XMAP215 of fission and budding yeasts is targeted to the γ-TuRC by the TACC ortholog Alp7 or Spc72 (Alfaro-Aco et al., 2017; Flor-Parra et al., 2018; Gunzelmann et al., 2018). Cooperation of MACET4 with γ-TuRC will have to be established by analyzing their colocalization at the nucleation sites. Considering colocalization of MACET4 with all microtubule nucleation sites in the interphase cells, both pathways are likely to cooperate. Overexpression of MACET4 in interphase cells does not have an impact on the frequency of microtubules nucleation events. It is possible that MACET4 nucleation activity is suppressed during interphase or masked by TPX2-, MOR1- or γ-TuRC-mediated nucleation mechanisms.

Despite promoting microtubule nucleation, TPX2 and MACET4 appear to have a different impact on microtubule dynamics: TPX2 reduces the frequency of catastrophe and increases the frequency of rescue leading to longer microtubules in the spindle (Reid et al., 2016; Roostalu et al., 2015; Wieczorek et al., 2015), whereas MACET4 promotes catastrophe *in vivo* and suppresses the rescue *in vitro*. Suppression of rescues *in vitro* could be indirect through depletion of free tubulin as the consequence of more-efficient microtubule nucleation. Partial depletion of the free tubulin pool could also be the reason for the overall suppression of microtubule polymerization in cells expressing MACET4 under control of its native promoter. Release of free tubulin during catastrophe would eventually enable nucleation of new or rescue of the existing microtubules (Fig. 3H). In this way MACET4 would ultimately cause formation of many short microtubules, which are typical for the phragmoplast (Segui-Simarro et al., 2007). Consistent with this hypothesis, knockout of *MACET4* leads to longer phragmoplasts. Our data also suggests that activity of MACET4 is modulated by the availability of free tubulin and by the cell cycle stage-dependent signaling processes.

Determining how MACET4 increases phragmoplast length would require careful analysis of phragmoplast microtubule dynamics in the mutant background. However, considering its strong nucleation activity, MACET4 could function in concentrating tubulin from all parts of the cytoplasm in the phragmoplast region. If this hypothesis is correct, then phragmoplast microtubules would be less dynamic in *mce4-1* strains. Furthermore, root apical meristem size was increased in *mce4-1* at 8°C through an as-yet-unknown mechanism.

In addition to promoting microtubule nucleation, MACET4 induces formation of asters from the non-polymerized tubulin *in vitro* in the manner that is similar to that mediated by centrosomes and TPX2 proteins (Gruss et al., 2002; Mitchison and Kirschner, 1984; Schatz et al., 2003). Asters formed in the reactions containing free tubulin, whereas mixing MACET4 with polymerized microtubules resulted in bundling and annealing. TPX2 has been proposed to form asters by bundling microtubules during nucleation (Schatz et al., 2003). Given the available evidence, induction of aster formation by MACET4 and by TPX2 is coupled with the microtubule nucleation activity. Tobacco histone H1 was also shown to induce aster formation (Nakayama et al., 2008); however, whether this activity is coupled to the nucleation is yet to be determined.

One important question is how does MACET4 promote microtubule nucleation? Our experiments demonstrate that, under control of the ubiquitin promoter, MACET4 localizes along the microtubule lattice and suppresses microtubule depolymerization in a TPX2-like manner. This means that a high concentration of MACET4 inhibits catastrophe. Under physiological protein levels, a high local concentration of MACET4 could be achieved through oligomerization, as MACET4 forms octamers *in vitro* and foci *in vivo*. These oligomers could function as the microtubule nucleation sites by inhibiting catastrophe.

A member of the MACET gene family, MACET1 (also known as CORD1), has been recently reported to play a role in the destabilization of cortical microtubules during formation of pits in the wall of xylem cells (Sasaki et al., 2017). The mechanism for microtubule destabilization by CORD1/MACET1 was proposed to be through inhibition of interaction between microtubules and the plasma membrane. Overexpression of CORD1/MACET1 resulted in microtubule wavering (Sasaki et al., 2017). We found that overexpression of MACET4 also induced wavering, but not the destabilization of microtubules. Instead microtubule depolymerization was suppressed. According to these findings, MACET4 and CORD1/MACET1 have distinct activities. Although we cannot exclude that decoration of microtubules by MACET4 in the overexpression situation causes wavering by out-competing the plasma-membrane linkers, the physiological meaning of this mechanism needs careful examination in cells expressing MACET4 under control of the native promoter. The density of microtubule labeling in this situation may not be sufficient to out-compete the interaction between microtubules and the membrane linkers unless these linker proteins bind to the same region on the microtubule lattice.

The direct binding of CORD1/MACET1 to microtubules has not been yet confirmed, but considering it shows a high conservation in the MACET4 microtubule-binding region, CORD1/MACET1 is likely a microtubule-binding protein. Experiments *in vivo* have demonstrated that CORD1/MACET1$^{200\text{-}505}$ decorates microtubules, whereas CORD1/MACET1$^{301\text{-}505}$ is cytoplasmic (Sasaki et al., 2017). By contrast, MACET4$^{287\text{-}518}$ could bind microtubules both

Journal of Cell Science (2019) 132, jcs232819. doi:10.1242/jcs.232819

in vitro and *in vivo* and perform all major activities of the full-length MACET4 *in vitro*. Thus, there appears to be a functional diversification amongst the MACET/CORD family members for the regulation of microtubule dynamics during cell division and vascular cell development. Detailed characterization of biochemical properties of MACET1 in the future would unravel the mechanisms underlying different activities of these proteins.

In conclusion, we identified and functionally characterized the first embryophyte-specific microtubule regulator in the phragmoplast, MACET4. MACET4 is a microtubule nucleation factor that accumulates at the distal zones of the phragmoplast, where microtubule nucleation takes place. Increase of the phragmoplast length in *mce4-1* strains indicates that MACET4 is essential for maintaining microtubule length in the phragmoplast. Our data together indicate that MACET4 facilitates microtubule turnover in the phragmoplast by maintaining the balance between nucleation and depolymerization. This work advances our knowledge on the mechanisms underlying phragmoplast assembly and paves the way for understanding phragmoplast evolution.

MATERIALS AND METHODS

Transient protein expression in *Nicotiana benthamiana*

Full-length *MACET4* cDNA was amplified by PCR from *Arabidopsis thaliana* Col-O leaf cDNA using primers MACET4fwdattB1 and MACET4revattB2 (Table S1) and cloned into Gateway binary vectors *pUBN* or *pUBC* (Grefen et al., 2010) harboring green fluorescent protein (GFP) for N- and C-terminal tagging, respectively. Plasmids were transformed into *Agrobacterium tumefaciens* strain GV3101. Transfected *A. tumefaciens* were grown overnight in 3.0 ml of YEB at 30°C, shaking at 200 rpm until optical density at 600 nm (OD_{600}) was between 0.5 and 1.0 for *MACET4* clones, and $OD_{600}\approx1.0$ for *p19* clone. Cells were collected by centrifugation at 3000 ***g*** for 5 min and washed two times with infiltration medium composed of 10 mM MES pH 5.6, 10 mM $MgCl_2$, and 200 µM Acetosyringone. After the second wash, bacteria were resuspended in 1.0 ml infiltration medium and incubated at room temperature for 2–5 h. Cells harboring *MACET4* constructs were mixed with cells harboring p19 at the ratio 1:1. *N. benthamiana* plants were grown at 21°C under a light cycle of 16 h light and 8 h dark for 3–4 weeks. Infiltration constructs were injected into the abaxial leaf side of either wild-type plants or *CaMV35S:Tub6-mCherry* stable transformants (Abe and Hashimoto, 2005). Leaves were imaged at 2–5 days after infiltration using a Leica SP8 or Leica SP8X confocal microscope. GFP was excited at 488 nm and mCherry was excited at 561 nm. To analyze colocalization of MACET4–GFP with the microtubule nucleation sites, the nucleation events were identified first on the TuB6–mCherry channel, and then MACET4–GFP channel was examined for the evidence of MACET4 accumulation at the nucleation site. Kymographs were constructed using ImageJ (Schindelin et al., 2012).

Inducible expression of MACET4 in BY2 cells

Full-length *MACET4* cDNA was amplified using primers MACET4 fwd attB2r and MACET4 rev attB3 (Table S1). An estradiol-inducible promoter was amplified from the *pMDC7* vector (Curtis and Grossniklaus, 2003) using primers pMDC7fwdattB4 and pMDC7revattB1r. Fragments were recombined into the gateway vector *pH7m34* together with *GFP* sequence so that the GFP was located on MACET4 N-terminus. Plasmids were transformed into *A. tumefaciens* strain LBA4404. BY-2 tissue culture cells were transformed with agrobacterium. Induction was performed with 5 µM estradiol for 48 h. Cells were imaged with a Leica SP8 confocal microscope.

Mutant analysis

A T-DNA insertional mutant from an *Arabidopsis* Biological Resource Center (ABRC) seed stock (SALK_070182.53.50) was genotyped for left border insertions using primers Salk070182fwd. RNA was extracted from seedlings and flowers of T-DNA lines homozygous for the left border insertion. cDNA was made with the MaximaH reverse transcriptase kit. cDNA flanking the insertion was amplified using primers complimentary to exon sequences: Salk079547fwd and Salk079547rev for *mce4-1*. cDNA upstream of the insertion was amplified using primers MACET4_fwd and MACET4 T_DNA_rev. cDNA downstream of the insertion was amplified using primers MACET4 T-DNA_fwd and MACET4_rev. cDNA was also amplified using the positive control primers, Salk073077_fwd and Salk073077_rev, which amplify a region on chromosome 3 within the *MACET1* gene (Table S1). The lack of amplification upstream, downstream and flanking the SALK_070182.53.50 insertion in *mce4-1* was interpreted as a knockout.

Analysis of root growth phenotype

Arabidopsis seeds were surface-sterilized with 75% ethanol with 0.05% (v/v) Triton X-100 for 15 min, 95% (v/v) ethanol with 0.05% Triton X-100 for 8 min. Seeds were then rinsed with 95% (v/v) ethanol, dried for 15 min, spread on half-strength MS-medium supplemented with 0.5% (w/v) sucrose, and incubated in 24 h light at 22°C. Two-day-old seedlings were transferred to half-strength MS plates and grown at 8°C for 4 weeks. Roots were imaged and root length was measured with ImageJ (Schindelin et al., 2012). Col-0 seedlings were used as a control. One-way ANOVA with Kruskal–Wallis test and Dunn's multiple comparison post-test were performed in GraphPad Prism version 5.01.

Analysis of phragmoplast size

Arabidopsis seeds were germinated on agar plates as above. Three-day-old seedlings of Col-0, *mce4-1* or *proMACET4:MACET4-GFP* were harvested and fixed for 1 h at room temperature in 3.7% paraformaldehyde, 50 mM PIPES, pH 6.8, 5 mM EGTA, 2 mM $MgSO_4$, 0.4% (v/v) Triton X-100 and 0.02% (w/v) glutaraldehyde. Roots were then washed three times for 5 min each time in PBST [PBS with 0.1% (v/v) Tween 20]. Cell walls were digested for 7 min at room temperature using an enzyme mixture containing 2% (w/v) Dricelase, 0.4 M Mannitol, 5 mM EGTA, 15 mM MES pH 5.0, 1 mM PMSF, and 10 µg/ml each of leupeptin and pepstatin A. Seedlings were rinsed twice for 5 min each time in PBST followed by in PBST supplemented with 2% (w/v) bovine serum albumin and 0.05% (w/v) NaN_3 for 30 min. Seedlings were incubated overnight at 4°C in rat primary anti-tubulin antibody YOL 1/34 (Fisher Scientific, 50174608) diluted 1:300 in the latter buffer. Following three washes for 2 h each in PBST, seedlings were incubated overnight at 4°C in secondary anti-rat-IgG Alexa Fluor 488-conjugated secondary antibody diluted 1:400 as above. After two washes for 30 min each in PBST, DNA was stained with a solution of DAPI (10 mg/ml) in PBST for 1 h at room temperature. Root tips were excised from the seedlings and mounted in Vectashield (Vector Labs). The coverslips were sealed using nail varnish. Phragmoplast microtubules in root tips were imaged with an SP8 confocal microscope. Phragmoplasts were measured with ImageJ and statistical analysis was performed with Graphpad Prism 5.1.

Generating native promoter lines

The *MACET4* promoter region, defined as the 2.3 kb region upstream of the *MACET4* transcriptional start site, was amplified using primers MACET4ProFWDattB1 and MACET4ProrevattB2 (Table S1). The promoter region was cloned into Gateway vector *pBI101G* upstream of the glucouronidase (GUS) reporter gene. Wild-type *Arabidopsis* plants were transformed using the floral dip method with *A. tumificiens* harboring *proMACET4:GUS* (Clough and Bent, 1998). GUS activity was detected in T2 generation by using a previously published procedure (Weigel and Glazebrook, 2002). To generate C-terminal GFP fusions, *proMACET4* and the open reading frame of *MACET4* were cloned together into the gateway vector *pMDC107* (Curtis and Grossniklaus, 2003). *mce4-1* T-DNA null mutant plants were transformed using floral dip method, and plants from the T2 generation were imaged. Membranes in roots were stained in 1 µM FM464 for 5 min and rinsed in water prior to imaging.

Purification of recombinant proteins

MACET4 full-length cDNA or fragments were amplified using primers listed in Table S1, and cloned into the *pGAT4* vector. A majority of the experiments were performed with non-labeled MACET4 in order to exclude potential artifacts associated with addition of the fluorescent protein. Protein

expression was conducted in *E. coli* strain BL21(DE3)Rosetta-2. Bacterial cultures were grown at 30°C until the OD_{600} reached ∼0.45 and induced with 1 mM IPTG for 3 h. Cells were collected by centrifugation at 3000 ***g*** for 5 min at room temperature. The pellet was resuspended in extraction buffer containing 50 mM HEPES pH 7.0, 300 mM NaCl, 20 mM imidazole, 30 mM β-mercaptoethanol, and 8 M urea. Cells were extracted overnight at room temperature. Debris was removed by centrifugation at 150,000 ***g*** for 2 h. Supernatant was poured into a nickel resin column and mixed for 10 min. Non-specifically bound proteins were removed with two washes of 40 mM imidazole with 4 M urea, and then three washes with 60 mM imidazole and 3 M urea. Bound proteins were eluted with 250 mM imidazole with 2 M urea. Eluate was concentrated and further purified using a Superdex 200 Increase column. Purified protein was dialyzed overnight at 4°C against buffer containing 20% (v/w) glycerol, 50 mM PIPES-KOH pH 6.8, 2 mM EGTA, 2 mM $MgSO_4$, 10 mM DTT and 50 mM KCl.

Microtubule co-sedimentation assay

Tubulin was purified from bovine brain using a published procedure (Castoldi and Popov, 2003). Microtubules were polymerized by adding 1 mM GTP, 10 µM Taxol and MTSB (50 mM PIPES-KOH, pH 6.8, 2 mM EGTA and 2 mM $MgSO_4$) to tubulin at final concentration of 40 µM. The mixture was incubated at 37°C for 30 min. Microtubules at 2 mg/ml microtubules in MTSB supplemented with 200 mM KCL were mixed with 2 µM *MACET4*, *MACET4*$^{1\text{-}127}$ or *MACET4*$^{287\text{-}518}$ and centrifuged at 100,000 ***g*** at 25°C for 10 min. 50 µl of supernatant was aspirated and mixed with 50 µl of 2× SDS-PAGE sample buffer. The remaining supernatant was discarded. The pellet was washed with 150 µl of warm MTSB supplemented with 0.5% (w/v) Tween-20 and resuspended in 200 µl of SDS-PAGE sample buffer. Protein samples were heated at 95°C for 5 min, then 20.0 µl of the samples were separated on a 12.5% (w/v) polyacrylamide resolving gel, 4% (w/v) polyacrylamide stacking gel at 30 mA. The gels were rinsed in deionized water, stained with colloidal Coomassie Brilliant Blue G-250 overnight and then distained with deionized water.

Bulk microtubule polymerization assays

To measure microtubule polymerization through a turbidimetric analysis, we prepared a reaction mixture containing 1 mM GTP, 20 µM tubulin and MACET4 in 120 µl of MTSB buffer. Reactions were mixed on ice in quartz cuvettes. Cuvettes were transferred from ice to a pre-warmed spectrophotometer chamber. The OD_{350} was measured at 350 nm every minute for 30 min or every 10 s for 15 min.

For measuring microtubule polymerization through sedimentation analysis, the reaction contained 1 mM GTP, 8 µM Tubulin, 0.05% (w/v) Tween-20 and MACET4 protein in MTSB, at a final volume of 100 µl. Reactions were incubated at 37°C for 20 min then centrifuged at 85,000 ***g*** at 37°C for 10 min. Supernatant was aspirated and the pellet was carefully washed with a 0.05% (w/v) solution of Tween 20 in deionized water at room temperature. The pellet was resuspended in 200 µl SDS-PAGE sample buffer and heated at 95°C for 5 min. 20 µl of protein was separated on a 12.5% (w/v) polyacrylamide resolving gel with a 4% (w/v) polyacrylamide stacking gel at 30 mA as described above. Band intensity was measured using ImageJ and charts were created with Graphpad Prism.

Stable microtubule 'seed' formation

Tubulin was labeled with NHS-Biotin, NHS-ATTO-488, or NHS-Rhodamine by following a previously published procedure (Peloquin et al., 2005). The mixtures of labeled and unlabeled tubulin were supplemented with 1 mM GMPCPP and 1 mM DTT in BRB80 buffer (80 mM PIPES-KOH pH 6.9, 1 mM $MgCl_2$ and 1 mM EGTA) to reach a final tubulin concentration of 40 µM. The mixture was incubated on ice for 5 min, clarified by centrifuging at 85,000 ***g*** for 5 min at 2°C, snap frozen in 10 µl aliquots and stored at −80°C. To polymerize tubulin, an aliquot of the seed mix was thawed in a 37°C water bath and supplemented with 5.0 µl of pre-warmed buffered glycerol. The reaction was incubated at 37°C for 20 min, and then gently resuspended in 150 µl of warm BRB80 plus 1 mM DTT, layered over a 60% glycerol cushion, pH 6.8, containing 10 µM Taxol, and centrifuged at 85,000 ***g*** for 5 min at 35°C. The glycerol cushion and supernatant were aspirated and the pellet was gently resuspended in 30 µl of warm BRB80 with 1 mM DTT. Seeds were further diluted in BRB80 plus 1 mM DTT as necessary.

Microtubule bundling assay

Microtubule seeds were made from the mixture of non-labeled and Rhodamine-labeled tubulin, or non-labeled and Atto488-labeled tubulin at the stoichiometric ratio of 3:1, as described above. Each reaction contained a mixture of 'red' and 'green' seeds in 20 µl BRB80. Reactions were incubated for 5 min at 37°C, then 8.0 µl of the reaction was placed on a 22×22 mm coverslip and imaged with a Leica TIRF DMI6000 microscope equipped with iLas 2 TIRF and FRAP system (Biovision Technologies). A minimum of 15 images were taken for each reaction. Seed encounters were scored manually and calculated as the percentage of total events.

Fixed fluorescent microtubules assay

A reaction mixture contained non-labeled and ATTO488-labeled tubulin at a ratio of 6:1 at a final concentration of 20 µM, and 1 mM GTP in 20 µl of MTSB. Reactions were mixed on ice then incubated for 20 min at 35°C. Microtubules were fixed by adding 100 µl of warm (35°C) MTSB supplemented with 0.5% (v/v) glutaraldehyde for 15 min. The reaction was further diluted in 600 µl of room temperature MTSB. 5 µl of reaction mix was added to a 22×22 mm coverslip and placed on a microscopy slide. Imaging was performed with a Leica TIRF microscope as above. A minimum of 15 images were taken for each reaction. Single microtubule lengths were measured using ImageJ and statistical analysis was performed with Graphpad Prism.

Microtubule nucleation and polymerization assay

Microtubule dynamics reconstitution experiments were performed using previously published procedures (Bieling et al., 2010). PEG-coated coverslips (MicroSurfaces, Inc.) were functionalized with 45 mg/ml solution NHS-biotin in dimethylformamide by sandwiching 80 µl of the biotin solution between two 22×22 mm coverslips and incubating at 75°C for 1 h. The coverslips were then rinsed twice in dimethylformamide and six times in RNase-free water. For functionalizing with NeutrAvidin, biotinylated coverslips were incubated for 10 min at room temperature with solution containing 50 µg/ml NeutrAvidin, 0.05% (w/v) K-casein, 80 mM PIPES (pH 6.8, KOH), 85 mM KCl, 85 mM KoAC, 0.25% (w/v) Brij-35, 4 mM $MgCl_2$, 1 mM EGTA, 1 mM GTP, 2 mM ATP and 10 mM β-mercaptoethanol. Coverslips were then rinsed in the same buffer, but without NeutrAvidin and K-casein, three times for 5 min each time, followed by in RNase-free water. Washed coverslips were blotted and air-dried.

To construct the reaction chamber, the functionalized coverslips and microscopy slides were cut in half along the long axis. Then, two pieces of double-sided tape were placed on the slide and the functionalized surface of the coverslip was placed perpendicular and face down on the tape so that edges of the coverslip extended over the edge of the slide, creating a 'landing stage' and chamber for buffer delivery. Nail varnish was used on the edge of the coverslip to secure the coverslip to the slide at the tape-attachment point. The chamber was rinsed twice with warm BRB80 plus DTT and then incubated for 5 min at room temperature with seeds prepared from ATTO488-labeled, biotin-labeled and non-labeled tubulin at the ratio 1:1:2. To flush the non-attached seeds, 80 µl of warm BRB80 plus DTT was added on one side of an extended coverslip and wicked with a paper towel from the other side. The chamber was then rinsed twice with 80 µl of ensemble buffer [80 mM PIPES-KOH, pH6.8, 85 mM KCl, 85 mM KoAC, 0.25% (w/v) Brij-35, 4 mM $MgCl_2$, 1 mM EGTA, 1 mM GTP, 2 mM ATP, 10 mM β-mercaptoethanol, 0.05% (w/v) β-casein, 0.1% (w/v) methylcellulose and Antifade system (250 nM glucose oxidase, 64 nM catalase, 40 mM D-glucose)].

Microtubule polymerization assays were performed on a microscope-stage pre-heated to 35°C. 5 µM tubulin and MACET4 were mixed on ice in ensemble buffer. 80 µl of ice-cold reaction solution was wicked through the chamber and imaging began immediately. Kymographs were made using the ImageJ kymograph plugin. Polymerization rates were calculated using Microsoft Excel. Statistical analysis was performed using Graphpad Prism.

Sequence analysis

Gene co-expression analysis was performed using ATTED-II (http://atted.jp/). Sequences were aligned using ClustalX (Thompson et al., 1997). The phylodendrogram was constructed using the Bootstrap/Jackknife method with PAUP 4.0 (Sinauer Associates). Bootstrap values were calculated from 1000 replicates; only groups with bootstrap scores of 60 or above were retained in the phylodendrogram. *Selaginella* MACET was used as an outgroup.

Acknowledgements

We thank ABRC for providing T-DNA seed stocks, Deirdre Fahy for technical assistance and Takashi Hashimoto for mCherry–TuB6 constructs.

Competing interests

The authors declare no competing or financial interests.

Author contributions

Conceptualization: S.S., A.S.; Methodology: S.S., A.S.; Validation: S.S., A.S.; Formal analysis: S.S., A.S.; Investigation: S.S., A.S.; Resources: A.S.; Data curation: S.S., A.S.; Writing - original draft: S.S., A.S.; Writing - review & editing: S.S., A.S.; Visualization: S.S., A.S.; Supervision: A.S.; Project administration: A.S.; Funding acquisition: A.S.

Funding

This work was supported by a Washington State University startup fund and the National Science Foundation (NSF)-CAREER award #1751204 to A.S.

Supplementary information

Supplementary information available online at
http://jcs.biologists.org/lookup/doi/10.1242/jcs.232819.supplemental

References

Abe, T. and Hashimoto, T. (2005). Altered microtubule dynamics by expression of modified alpha-tubulin protein causes right-handed helical growth in transgenic Arabidopsis plants. *Plant J.* **43**, 191-204. doi:10.1111/j.1365-313X.2005.02442.x

Alfaro-Aco, R., Thawani, A. and Petry, S. (2017). Structural analysis of the role of TPX2 in branching microtubule nucleation. *J. Cell Biol.* **216**, 983-997. doi:10.1083/jcb.201607060

Bajer, A. (1968). Fine structure studies on phragmoplast and cell plate formation. *Chromosoma* **24**, 383-417. doi:10.1007/BF00285016

Becker, W. A. (1938). Recent investigations in vivo on the division of plant cells. *Bot. Rev.* **4**, 446-472. doi:10.1007/BF02872541

Bieling, P., Telley, I. A., Hentrich, C., Piehler, J. and Surrey, T. (2010). Fluorescence microscopy assays on chemically functionalized surfaces for quantitative imaging of microtubule, motor, and +TIP dynamics. *Methods Cell Biol.* **95**, 555-580. doi:10.1016/S0091-679X(10)95028-0

Brunet, S., Sardon, T., Zimmerman, T., Wittmann, T., Pepperkok, R., Karsenti, E. and Vernos, I. (2004). Characterization of the TPX2 domains involved in microtubule nucleation and spindle assembly in Xenopus egg extracts. *Mol. Biol. Cell* **15**, 5318-5328. doi:10.1091/mbc.e04-05-0385

Buschmann, H. and Zachgo, S. (2016). The evolution of cell division: from streptophyte algae to land plants. *Trends Plant Sci.* **21**, 872-883. doi:10.1016/j.tplants.2016.07.004

Castoldi, M. and Popov, A. V. (2003). Purification of brain tubulin through two cycles of polymerization–depolymerization in a high-molarity buffer. *Protein Expression Purif.* **32**, 83-88. doi:10.1016/S1046-5928(03)00218-3

Cleary, A. L. and Smith, L. G. (1998). The Tangled1 gene is required for spatial control of cytoskeletal arrays associated with cell division during maize leaf development. *Plant Cell* **10**, 1875-1888. doi:10.1105/tpc.10.11.1875

Clough, S. J. and Bent, A. F. (1998). Floral dip: a simplified method for Agrobacterium-mediated transformation of Arabidopsis thaliana. *Plant J.* **16**, 735-743. doi:10.1046/j.1365-313x.1998.00343.x

Cook, M. E. (2004). Cytokinesis in coleochaete orbicularis (Charophyceae): an ancestral mechanism inherited by plants. *Am. J. Bot.* **91**, 313-320. doi:10.3732/ajb.91.3.313

Cook, M. E., Graham, L. E. and Lavin, C. A. (1998). Cytokinesis and nodal anatomy in the charophycean green alga Chara zeylanica. *Protoplasma.* **203**, 65-74. doi:10.1007/BF01280588

Curtis, M. D. and Grossniklaus, U. (2003). A gateway cloning vector set for high-throughput functional analysis of genes in planta. *Plant Physiol.* **133**, 462-469. doi:10.1104/pp.103.027979

Cutler, S. R. and Ehrhardt, D. W. (2002). Polarized cytokinesis in vacuolate cells of Arabidopsis. *Proc. Natl. Acad. Sci. USA* **99**, 2812-2817. doi:10.1073/pnas.052712299

Flor-Parra, I., Iglesias-Romero, A. B. and Chang, F. (2018). The XMAP215 Ortholog Alp14 promotes microtubule nucleation in fission yeast. *Curr. Biol.* **28**, 1681. doi:10.1016/j.cub.2018.04.008

Grefen, C., Donald, N., Hashimoto, K., Kudla, J., Schumacher, K. and Blatt, M. R. (2010). A ubiquitin-10 promoter-based vector set for fluorescent protein tagging facilitates temporal stability and native protein distribution in transient and stable expression studies. *Plant J.* **64**, 355-365. doi:10.1111/j.1365-313X.2010.04322.x

Gruss, O. J., Carazo-Salas, R. E., Schatz, C. A., Guarguaglini, G., Kast, J., Wilm, M., Le Bot, N., Vernos, I., Karsenti, E. and Mattaj, I. W. (2001). Ran induces spindle assembly by reversing the inhibitory effect of importin alpha on TPX2 activity. *Cell* **104**, 83-93. doi:10.1016/S0092-8674(01)00193-3

Gruss, O. J., Wittmann, M., Yokoyama, H., Pepperkok, R., Kufer, T., Silljé, H., Karsenti, E., Mattaj, I. W. and Vernos, I. (2002). Chromosome-induced microtubule assembly mediated by TPX2 is required for spindle formation in HeLa cells. *Nat. Cell Biol.* **4**, 871-879. doi:10.1038/ncb870

Gunzelmann, J., Rüthnick, D., Lin, T.-C., Zhang, W. L., Neuner, A., Jäkle, U. and Schiebel, E. (2018). The microtubule polymerase Stu2 promotes oligomerization of the gamma-TuSC for cytoplasmic microtubule nucleation. *eLife* **7**, e39932. doi:10.7554/eLife.39932

Hashimoto, T. (2013). A ring for all: gamma-tubulin-containing nucleation complexes in acentrosomal plant microtubule arrays. *Curr. Opin. Plant Biol.* **16**, 698-703. doi:10.1016/j.pbi.2013.09.002

Hepler, P. K. and Jackson, W. T. (1968). Microtubules and early stages of cell-plate formation in the endosperm of *Haemanthus katherinae* Baker. *J. Cell Biol.* **38**, 437-446. doi:10.1083/jcb.38.2.437

Hush, J. M., Wadsworth, P., Callaham, D. A. and Hepler, P. K. (1994). Quantification of microtubule dynamics in living plant-cells using fluorescence redistribution after photobleaching. *J. Cell Sci.* **107**, 775-784.

Kawamura, E., Himmelspach, R., Rashbrooke, M. C., Whittington, A. T., Gale, K. R., Collings, D. A. and Wasteneys, G. O. (2006). MICROTUBULE ORGANIZATION 1 regulates structure and function of microtubule arrays during mitosis and cytokinesis in the Arabidopsis root. *Plant Physiol.* **140**, 102-114. doi:10.1104/pp.105.069989

Leliaert, F., Verbruggen, H. and Zechman, F. W. (2011). Into the deep: new discoveries at the base of the green plant phylogeny. *BioEssays* **33**, 683-692. doi:10.1002/bies.201100035

Lindeboom, J. J., Nakamura, M., Hibbel, A., Shundyak, K., Gutierrez, R., Ketelaar, T., Emons, A. M. C., Mulder, B. M., Kirik, V. and Ehrhardt, D. W. (2013). A mechanism for reorientation of cortical microtubule arrays driven by microtubule severing. *Science* **342**, 1245533. doi:10.1126/science.1245533

Martinez, P., Luo, A., Sylvester, A. and Rasmussen, C. G. (2017). Proper division plane orientation and mitotic progression together allow normal growth of maize. *Proc. Natl. Acad. Sci. USA* **114**, 2759-2764. doi:10.1073/pnas.1619252114

McMichael, C. M. and Bednarek, S. Y. (2013). Cytoskeletal and membrane dynamics during higher plant cytokinesis. *New Phytol.* **197**, 1039-1057. doi:10.1111/nph.12122

Mitchison, T. and Kirschner, M. (1984). Microtubule assembly nucleated by isolated centrosomes. *Nature* **312**, 232-237. doi:10.1038/312232a0

Nakayama, T., Ishii, T., Hotta, T. and Mizuno, K. (2008). Radial microtubule organization by histone H1 on nuclei of cultured tobacco BY-2 cells. *J. Biol. Chem.* **283**, 16632-16640. doi:10.1074/jbc.M705764200

Otegui, M. S., Verbrugghe, K. J. and Skop, A. R. (2005). Midbodies and phragmoplasts: analogous structures involved in cytokinesis. *Trends Cell Biol.* **15**, 404-413. doi:10.1016/j.tcb.2005.06.003

Pastuglia, M., Azimzadeh, J., Goussot, M., Camilleri, C., Belcram, K., Evrard, J. L., Schmit, A. C., Guerche, P. and Bouchez, D. (2006). Gamma-tubulin is essential for microtubule organization and development in Arabidopsis. *Plant Cell* **18**, 1412-1425. doi:10.1105/tpc.105.039644

Peloquin, J., Komarova, Y. and Borisy, G. (2005). Conjugation of fluorophores to tubulin. *Nat. Methods* **2**, 299-303. doi:10.1038/nmeth0405-299

Rasmussen, C. G., Sun, B. and Smith, L. G. (2011). Tangled localization at the cortical division site of plant cells occurs by several mechanisms. *J. Cell Sci.* **124**, 270-279. doi:10.1242/jcs.073676

Reid, T. A., Schuster, B. M., Mann, B. J., Balchand, S. K., Plooster, M., McClellan, M., Coombes, C. E., Wadsworth, P. and Gardner, M. K. (2016). Suppression of microtubule assembly kinetics by the mitotic protein TPX2. *J. Cell Sci.* **129**, 1319-1328. doi:10.1242/jcs.178806

Roostalu, J., Cade, N. I. and Surrey, T. (2015). Complementary activities of TPX2 and chTOG constitute an efficient importin-regulated microtubule nucleation module. *Nat. Cell Biol.* **17**, 1422-1434. doi:10.1038/ncb3241

Samuels, A. L., Giddings, T. H. and Staehelin, L. A. (1995). Cytokinesis in tobacco BY-2 and root-tip cells: a new model of cell plate formation in higher-plants. *J. Cell Biol.* **130**, 1345-1357. doi:10.1083/jcb.130.6.1345

Sasaki, T., Fukuda, H. and Oda, Y. (2017). CORTICAL MICROTUBULE DISORDERING1 is required for secondary cell wall patterning in Xylem vessels. *Plant Cell* **29**, 3123-3139. doi:10.1105/tpc.17.00663

Schatz, C. A., Santarella, R., Hoenger, A., Karsenti, E., Mattaj, I. W., Gruss, O. J. and Carazo-Salas, R. E. (2003). Importin alpha-regulated nucleation of microtubules by TPX2. *EMBO J.* **22**, 2060-2070. doi:10.1093/emboj/cdg195

Schindelin, J., Arganda-Carreras, I., Frise, E., Kaynig, V., Longair, M., Pietzsch, T., Preibisch, S., Rueden, C., Saalfeld, S., Schmid, B. et al. (2012). Fiji: an

open-source platform for biological-image analysis. *Nat. Methods* **9**, 676-682. doi:10.1038/nmeth.2019

Schmidt, S. and Smertenko, A. (2016). 2016 ASCB annual meeting abstracts; P981: characterization of a plant-specific microtubule-nucleating protein MACERATOR. *Mol. Biol. Cell* **27**, 3947-3947. doi:10.1091/mbc.e16-10-0736.

Segui-Simarro, J. M., Austin, J. R., II, White, E. A. and Staehelin, L. A. (2004). Electron tomographic analysis of somatic cell plate formation in meristematic cells of Arabidopsis preserved by high-pressure freezing. *Plant Cell* **16**, 836-856. doi:10.1105/tpc.017749

Segui-Simarro, J. M., Otegui, M. S., Austin, J. R., II and Staehelin, L. A. (2007). Plant cytokinesis - insights gained from electron tomography studies. In *Cell Division Control in Plants*, Vol. 9 (ed. D. P. S. Verma and Z. Hong), pp. 251-287. Berlin Heidelberg: Springer-Verlag.

Smertenko, A. P., Piette, B. and Hussey, P. J. (2011). The origin of phragmoplast asymmetry. *Curr. Biol.* **21**, 1924-1930. doi:10.1016/j.cub.2011.10.012

Smertenko, A., Assaad, F., Baluška, F., Bezanilla, M., Buschmann, H., Drakakaki, G., Hauser, M.-T., Janson, M., Mineyuki, Y., Moore, I. et al. (2017). Plant cytokinesis: terminology for structures and processes. *Trends Cell Biol.* **27**, 885-894. doi:10.1016/j.tcb.2017.08.008

Smertenko, A., Hewitt, S. L., Jacques, C. N., Kacprzyk, R., Liu, Y., Marcec, M. J., Moyo, L., Ogden, A., Oung, H. M., Schmidt, S. et al. (2018). Phragmoplast microtubule dynamics - a game of zones. *J. Cell Sci.* **131**, jcs203331. doi:10.1242/jcs.203331

Smith, L. G., Gerttula, S. M., Han, S. C. and Levy, J. (2001). TANGLED1: a microtubule binding protein required for the spatial control of cytokinesis in maize. *J. Cell Biol.* **152**, 231-236. doi:10.1083/jcb.152.1.231

Thawani, A., Kadzik, R. S. and Petry, S. (2018). XMAP215 is a microtubule nucleation factor that functions synergistically with the gamma-tubulin ring complex. *Nat. Cell Biol.* **20**, 575. doi:10.1038/s41556-018-0091-6

Thompson, J. D., Gibson, T. J., Plewniak, F., Jeanmougin, F. and Higgins, D. G. (1997). The CLUSTAL_X windows interface: flexible strategies for multiple sequence alignment aided by quality analysis tools. *Nuc. Acids Res.* **25**, 4876-4882. doi:10.1093/nar/25.24.4876

Twell, D., Park, S. K., Hawkins, T. J., Schubert, D., Schmidt, R., Smertenko, A. and Hussey, P. J. (2002). MOR1/GEM1 has an essential role in the plant-specific cytokinetic phragmoplast. *Nat. Cell Biol.* **4**, 711-714. doi:10.1038/ncb844

Ueda, K., Sakaguchi, S., Kumagai, F., Hasezawa, S., Quader, H. and Kristen, U. (2003). Development and disintegration of phragmoplasts in living cultured cells of a GFP::TUA6 transgenic Arabidopsis thaliana plant. *Protoplasma* **220**, 111-118. doi:10.1007/s00709-002-0049-0

Vos, J. W., Pieuchot, L., Evrard, J.-L., Janski, N., Bergdoll, M., de Ronde, D., Perez, L. H., Sardon, T., Vernos, I. and Schmit, A.-C. (2008). The plant TPX2 protein regulates prospindle assembly before nuclear envelope breakdown. *Plant Cell* **20**, 2783-2797. doi:10.1105/tpc.107.056796

Vyplelová, P., Ovečka, M., Komis, G. and Šamaj, J. (2018). Advanced microscopy methods for bioimaging of mitotic microtubules in plants. *Methods Cell Biol.* **145**, 129-158. doi:10.1016/bs.mcb.2018.03.019

Walker, K. L., Müller, S., Moss, D., Ehrhardt, D. W. and Smith, L. G. (2007). Arabidopsis TANGLED identifies the division plane throughout mitosis and cytokinesis. *Curr. Biol.* **17**, 1827-1836. doi:10.1016/j.cub.2007.09.063

Wasteneys, G. O. (2002). Microtubule organization in the green kingdom: chaos or self-order? *J. Cell Sci.* **115**, 1345-1354.

Weigel, D. and Glazebrook, J. (2002). Whole mount Gus staining. In *Arabidopsis: A Laboratory Manual*, p. 243. Cold Spring Harbor Laboratory Press.

Wieczorek, M., Bechstedt, S., Chaaban, S. and Brouhard, G. J. (2015). Microtubule-associated proteins control the kinetics of microtubule nucleation. *Nat. Cell Biol.* **17**, 907-916. doi:10.1038/ncb3188

Wittmann, T., Boleti, H., Antony, C., Karsenti, E. and Vernos, I. (1998). Localization of the kinesin-like protein Xklp2 to spindle poles requires a leucine zipper, a microtubule-associated protein, and dynein. *J. Cell Biol.* **143**, 673-685. doi:10.1083/jcb.143.3.673

Yasuhara, H., Sonobe, S. and Shibaoka, H. (1993). Effects of taxol on the development of the cell plate and of the phragmoplast in tobacco BY-2 cells. *Plant Cell Physiol.* **34**, 21-29.